NEUROIMMUNOLOGY

Meningeal regulatory T cells inhibit nociception in female mice

Élora Midavaine[1], Beatriz C. Moraes[1], Jorge Benitez[1], Sian R. Rodriguez[1], Joao M. Braz[1], Nathan P. Kochhar[1], Walter L. Eckalbar[1], Lin Tian[2], Ana I. Domingos[3], John E. Pintar[4], Allan I. Basbaum[1]*†, Sakeen W. Kashem[5,6]*†

T cells have emerged as orchestrators of pain amplification, but the mechanism by which T cells control pain processing is unresolved. We found that regulatory T cells (T_{reg} cells) could inhibit nociception through a mechanism that was not dependent on their ability to regulate immune activation and tissue repair. Site-specific depletion or expansion of meningeal T_{reg} cells (mT_{reg} cells) in mice led to female-specific and sex hormone–dependent modulation of mechanical sensitivity. Specifically, mT_{reg} cells produced the endogenous opioid enkephalin that exerted an antinociceptive action through the delta opioid receptor expressed by $MrgprD^+$ sensory neurons. Although enkephalin restrains nociceptive processing, it was dispensable for T_{reg} cell–mediated immunosuppression. Thus, our findings uncovered a sexually dimorphic immunological circuit that restrains nociception, establishing T_{reg} cells as sentinels of pain homeostasis.

Pain prevalence is higher in women across multiple conditions, and chronic pain severity is frequently altered during gender affirming hormonal therapy (*1*). Although there is evidence that T cells contribute to sexually dimorphic pain processing, the exact mechanisms remain unclear (*2*). Regulatory T cells (T_{reg} cells) are a subset of $CD4^+$ T cells defined by the expression of the master transcriptional regulator FOXP3, which is encoded by a gene found on the X chromosome. In addition to their critical function in restraining inflammation, T_{reg} cells are major contributors of tissue reparative and supportive functions (*3*, *4*). However, it is not known whether and how T_{reg} cells directly alter neuronal activity to modulate nociception, independently of their immunomodulatory functions (*5*, *6*). In this study, we examined the role of T_{reg} cells in regulating pain sensing in mice.

Sex-specific suppression of nociceptive thresholds by meningeal T_{reg} cells

We focused on T_{reg} cells within nervous system tissue, localized to the meninges of the central nervous system (CNS) and to the leptomeninges of dorsal root ganglia (DRGs). As previously reported, we observed a more pronounced localization of T_{reg} cells in the lumbar and sacral segments of the spinal cord (SC) meninges, and T_{reg} cells were observed along meningeal nerve fibers, including fibers expressing the protein isolectin $B4^+$ ($IB4^+$) that marks nonpeptidergic sensory neurons (Fig. 1A and fig. S1A) (*7*). In the DRGs, T_{reg} cells predominated in the leptomeninges, with sparse presence within the DRG parenchyma (Fig. 1B and fig. S1B). We quantified the numbers of nonvascular-tissue T_{reg} cells in various organs within the nervous and lymphoid systems (Fig. 1C). We further refer to the SC meningeal and DRG leptomeningeal T_{reg} cells as meningeal T_{reg} cells (mT_{reg} cells) (Fig. 1C). We observed minimal localization of T_{reg} cells in peripheral nerves or CNS parenchyma, as previously noted (*8*), and observed nearly equivalent numbers of tissue T_{reg} cells in male and female mice across tissues (Fig. 1D and fig. S1, C and D).

To assess the feasibility of site-specific depletion of mT_{reg} cells, we performed intrathecal (IT) injections of pegylated diphtheria toxin (pegDT) in *Foxp3*-DTR mice expressing the diphtheria toxin receptor (DTR) under the control of the *Foxp3* promoter, leading to T_{reg} cell–specific cell death on toxin administration (*9*). Although an IT injection of Evans blue rapidly spreads through the meninges, DRGs, brain, and into the draining lymph nodes, pegylated fluorescently labeled molecules remain restricted to the SC meninges and to the DRGs (fig. S2, A and B). Consistently, a single dose of pegDT IT selectively depleted >90% of SC and DRG mT_{reg} cells in both male and female mice but spared T_{reg} cells located in all other organs (Fig. 1, E and F, and fig. S2C). *Foxp3*-DTR mice subjected to repeated pegDT IT did not exhibit weight loss, splenomegaly, or mortality that developed after systemic autoimmunity in *Foxp3*-DTR mice that received repeated intraperitoneal (IP) injections of diphtheria toxin (DT) (fig. S2, D to G). Thus, IT injections of pegDT allow for site-selective depletion of mT_{reg} cells while avoiding systemic inflammation.

We evaluated behavioral outcomes in mice after mT_{reg} cell depletion in response to pain mediated by mechanosensitive unmyelinated and myelinated primary afferent nerve fibers. A single dose of pegDT IT decreased mechanical nociceptive thresholds in naïve female, but not male, *Foxp3*-DTR mice (Fig. 1, G and H). Mechanical pain thresholds in C57BL/6 mice treated with pegDT IT and in *Foxp3*-DTR mice treated with vehicle IT did not differ (fig. S3A), which indicates that neither pegDT nor IT injections alone caused increased pain hypersensitivity. In addition, we assessed mice for noxious heat sensitivity (mediated by $Trpv1^+$ nociceptors), cold sensitivity ($Trpm8^+$ nociceptors), pinprick (Aδ fibers), and brush responses (Aβ fibers). Depletion of mT_{reg} cells selectively induced mechanical hypersensitivity in female mice, but in neither sex did it affect other sensory modalities or motor function (Fig. 1I and fig. S3, A to H). We concluded that mT_{reg} cells suppress mechanical nociceptive thresholds in a sex-dependent manner in uninjured mice.

mT_{reg} cells alleviate injury-induced mechanical hypersensitivity independently of tissue repair

We investigated whether mT_{reg} cells could suppress nociception after nerve injury. We used a well-established spared nerve injury (SNI) model of neuropathic pain, in which transection and ligation of two branches of the sciatic nerve induces permanent and unremitting mechanical hypersensitivity (Fig. 2, A and B). SNI also produces a nonhealing neuroma 4 weeks after the injury (*10*). Additionally, meninges are physically segregated from peripheral nerves through tight junctions. Thus, because tissue injury cannot be repaired to resolve pain, this model allows of assessment of mT_{reg} cell function in nociception specifically. After SNI, we observed no changes in meningeal T_{reg} cell numbers (fig. S4A). Because mice with SNI respond to mechanical stimuli at the limit of detection with von Frey filaments, we used the percent response method with the lightest available filament (*11*). This approach assesses pain sensitivity by measuring how often mice react to the most innocuous available mechanical stimuli. Nociceptive responses were increased in female mice with mT_{reg} cell depletion after SNI, but this was not observed in males (Fig. 2, C and D).

Our data indicated that mT_{reg} cells may decrease pain sensing; therefore, we investigated whether expanding mT_{reg} cells could alleviate mechanical hypersensitivity after SNI. T_{reg} cells express the high-affinity interleukin-2 (IL-2) receptor, and administrations of low doses of IL-2 can effectively expand T_{reg} cells in mice—a therapeutic approach used to treat autoimmune diseases in humans (*12*). IT injections of low-dose IL-2 selectively expanded mT_{reg} cells

[1]Department of Anatomy, University of California San Francisco, San Francisco, CA, USA. [2]Max Planck Florida Institute for Neuroscience, Jupiter, FL, USA. [3]Department of Physiology, Anatomy and Genetics, University of Oxford, Oxford, UK. [4]Department of Neuroscience and Cell Biology, Rutgers Robert Wood Johnson Medical School, Piscataway, NJ, USA. [5]Department of Dermatology, University of California San Francisco, San Francisco, CA, USA. [6]Dermatology, Veterans Affairs Medical Center, San Francisco, CA, USA.
*Corresponding author. Email: sakeen.kashem@ucsf.edu (S.W.K.); allan.basbaum@ucsf.edu (A.I.B.)
†These authors contributed equally to this work

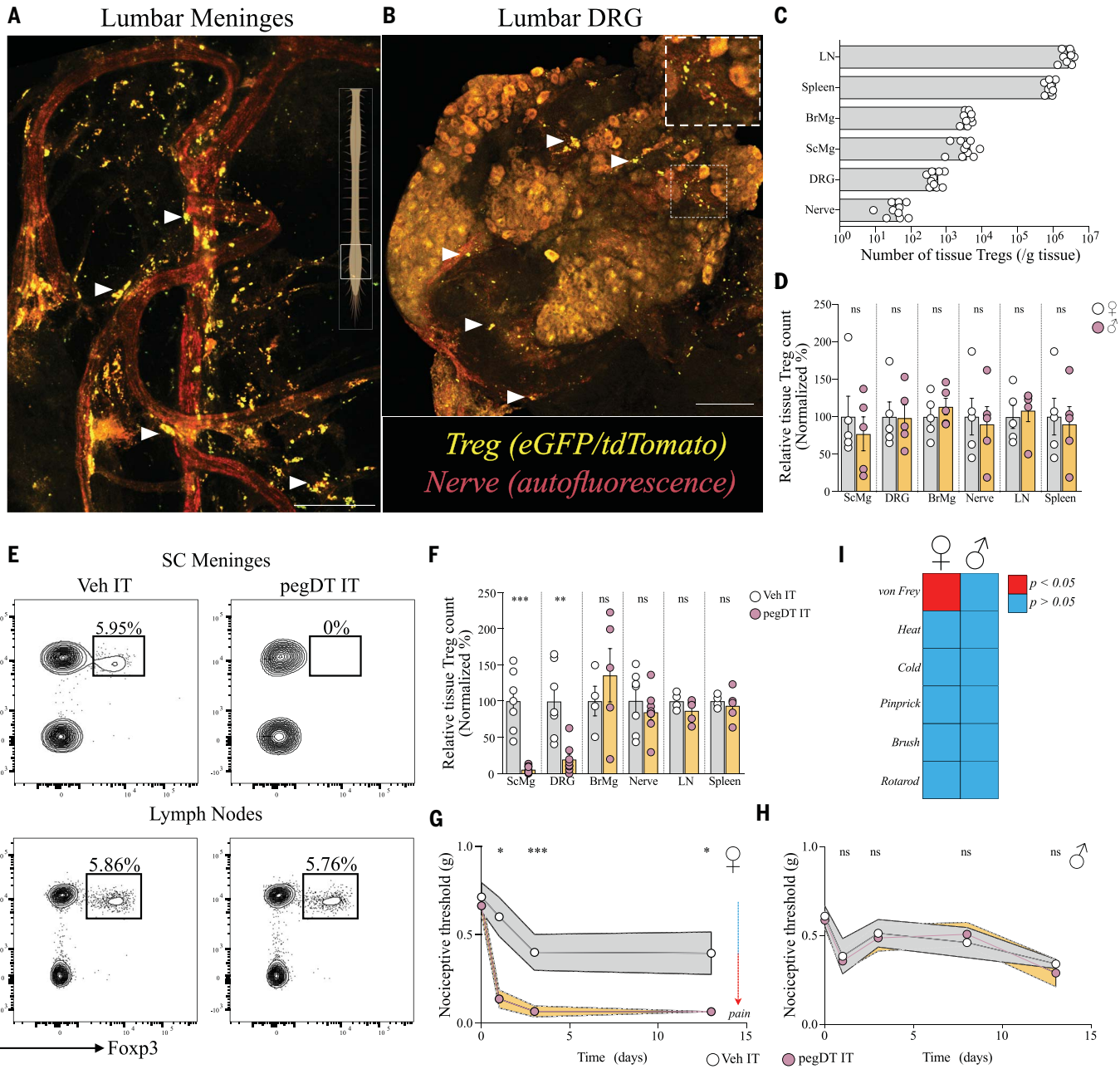

Fig. 1. Sex-selective suppression of mechanical pain hypersensitivity by mT_{reg} cells. (**A** and **B**) Representative (n = 5) whole-mount maximum projection confocal microscopy image of the lumbar SC meninges (A) and DRGs (B) showing T_{reg} cells (green-red: yellow) and nerves (autofluorescence, red) in *Foxp3*$^{eGFP\text{-}Cre\text{-}ERT2}$;*Rosa26*^{tdTomato} reporter mice. Inset in (B) shows DRG magnification. Scale bars, 100 μm (A) and 150 μm (B). Arrowheads indicate T_{reg} cells. (**C**) Total number of weight-adjusted tissue T_{reg} cells across organs in both sexes combined; n = 9 to 10 mice per organ. (**D**) Relative number of tissue T_{reg} cells from male (white; n = 5) mice and female (black; n = 5) mice per organ. 100% represents mean number of female T_{reg} cells per organ. Comparison is made between the sexes in each individual organ. (**E**) Representative concatenated flow cytometry (n = 5) plots of tissue T_{reg} cells after a single IT injection of 20 ng of pegDT. Gating strategy is provided in fig. S1. (**F**) Relative quantifications of tissue T_{reg} cell depletion 2 days after a single IT pegDT injection across organs; n = 4 to 8 mice per organ. 100% represents mean number of tissue T_{reg} cells in IT vehicle-injected mice per organ. (**G** and **H**) Nociceptive thresholds measured in *Foxp3*-DTR mice using von Frey filaments before (day 0) and after a single dose of 20 ng of IT pegDT or vehicle in female (n = 9 mice per group) (G) or male (n = 13 to 15 mice per group) mice (H). Downward-pointing arrow represents increased pain sensitivity. (**I**) Summary of behavioral differences comparing IT pegDT- and control-injected female and male mice. In graphs (C), (D), and (F), individual data points show data for one mouse, and bars show means ± SEMs. In graphs (G) and (H), individual data points show means ± SEMs. Statistics were calculated by unpaired two-tailed Mann-Whitney test [(D) and (F)] or two-way analysis of variance (ANOVA) with Sidak's test for multiple comparisons [(G) and (H)]. ScMg, spinal cord meninges; BrMg, brain meninges; LN, lymph nodes; Veh, vehicle. ns, not significant; *P < 0.05; **P < 0.01; ***P < 0.001.

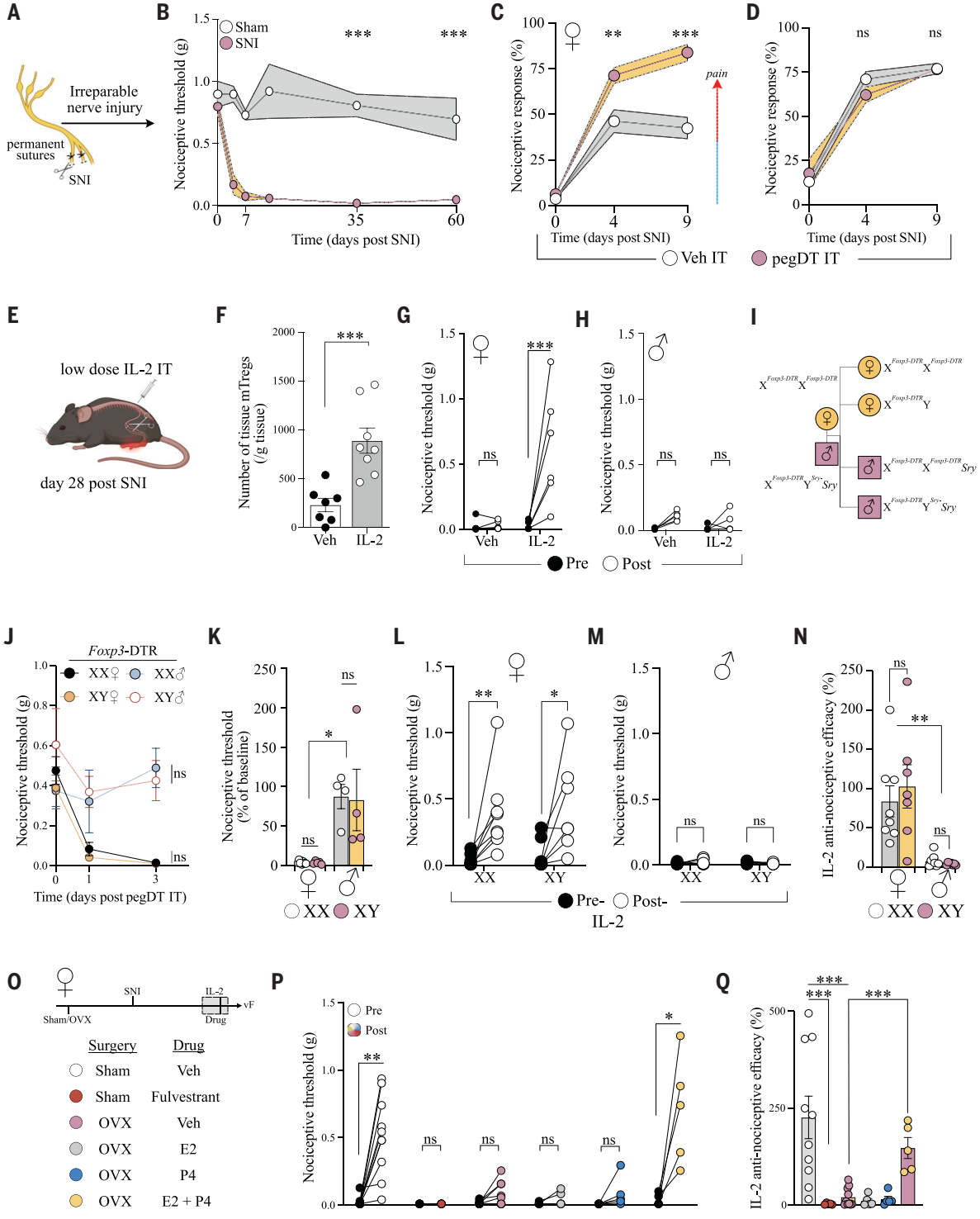

Fig. 2. mT_{reg} cells control nociception dependent on sex hormones and independent of tissue repair. (**A**) Schematic representation of the SNI surgery. (**B**) Long-term assessment of mechanical pain thresholds in mice after SNI surgery (both sexes combined, no difference between the sexes); *n* = 7 to 8 mice per group. (**C** and **D**) Percent response to 0.008 g of von Frey filament in mice with SNI (day 0) and treated with IT pegDT or vehicle every 4 days. *n* = 8 per group for females and 9 to 10 per group for males. Upward-pointing arrow represents increased pain responsiveness. (**E**) Schematic representation of mT_{reg} cell expansion in mice 4 weeks after SNI by three IT injections of low-dose IL-2 (0.1 μg). (**F**) Total mT_{reg} cell number in meninges after low-dose IL-2 or vehicle IT injections (both sexes combined, no significant differences between the sexes); *n* = 7 to 8 mice per group. (**G** and **H**) Nociceptive thresholds of female (*n* = 7 to 12 mice per group) (G) and male (*n* = 5 mice per group) (H) mice given low-dose IL-2 or vehicle IT 4 weeks after SNI. (**I**) Schematic representation of the mating strategy of FCG *Foxp3*-DTR mice, demonstrating resulting XX and XY females and XX and XY male mice. (**J**) Nociceptive thresholds of FCG *Foxp3*-DTR female and male mice after a single IT pegDT injection. *n* = 5 to 9 per group for females and 4 per group for males. (**K**) Percent baseline nociceptive thresholds is determined as post–pegDT injection threshold divided by preinjection, basal mechanical threshold in male and female mice

with XX (white) or XY (pink) chromosomes. *N* = 4 to 9 mice per group. (**L** and **M**) Nociceptive thresholds of WT FCG female (*n* = 7 to 8 mice per group) (L) and male (*n* = 7 to 8 mice per group) (M) mice after low-dose IL-2 injections 4 weeks after SNI. (**N**) Antinociceptive efficacy determined as post–IL-2 injection threshold divided by preinjury, basal mechanical threshold in male and female mice with XX (white) or XY (pink) chromosomes. (**O**) Outline of experiment. (**P**) Nociceptive thresholds of sham or ovariectomized (OVX) female mice after low-dose IL-2 injections 4 weeks after SNI, and injected with either vehicle, fulvestrant, estrogen (E2), progesterone (P4), or both estrogen and progesterone; 5 to 10 mice per group. (**Q**) Antinociceptive efficacy determined as post–IL-2 injection threshold divided by preinjury mechanical threshold in female mice with hormone manipulation. In graphs (F), (G), (H), (K), (L), (M), (N), (P), and (Q), individual data points show data for one mouse, and bars show means ± SEMs. In graphs (B), (C), (D), and (J), individual data points show means ± SEMs. Statistics were calculated by two-way ANOVA with Sidak's test for multiple comparisons [(B), (C), (D), and (J)], unpaired two-tailed Mann-Whitney test (F), Wilcoxon matched-pairs signed rank test [(G), (H), (L), (M), and (O)], or Kruskal-Wallis with Dunn's multiple comparisons test [(K), (N), and (P)]. ns, not significant; **P* < 0.05; ***P* < 0.01; ****P* < 0.001.

in both male and female mice (Fig. 2, E and F, and fig. S4B). Although mT_{reg} cell expansion promoted antinociception in female mice post-SNI, it did not exhibit a similar effect in males (Fig. 2, G and H). IT injections of IL-2 in uninjured mice did not increase nociceptive thresholds (fig. S4, C and D). In addition, mT_{reg} cell expansion did not alter noxious heat and cold sensitivity in mice with SNI and did not induce motor impairment (fig. S4, E to J). Thus, the expansion of mT_{reg} cells selectively alleviated mechanical hypersensitivity independently of their ability to repair tissue injury.

Gonadal hormones control the antinociceptive function of mT_{reg} cells

There are reports of altered X chromosome inactivation during inflammatory state in females (*13*, *14*), which suggests that differences in *Foxp3* through sex chromosome dosage may contribute to female-specific function mT_{reg} cells in nociceptive regulation. We used the four core genotypes (FCG) mouse model in which gonadal sex is independent of sex chromosomes (*15*). FCG mice harbor a deletion in the sex-determining region Y gene (*Sry*) on the Y chromosome and instead feature an autosomal transgenic insertion of *Sry*. This genetic configuration makes it possible to distinguish sex chromosome dose influence from the contribution of gonadal hormones (Fig. 2I). mT_{reg} cell depletion in *Foxp3*-DTR mice crossed with FCG mice demonstrated that both XX and XY gonadal females, but not males, exhibited increased sensitivity after mT_{reg} cell depletion. This revealed that gonadal hormones, but not sex chromosomes, mediated the mT_{reg} cell suppression of mechanical nociceptive thresholds in the absence of nerve injury (Fig. 2, J and K). XX and XY chromosome gonadal female mice, but not male mice, displayed intact mT_{reg} cell expansion–mediated alleviation of SNI-induced mechanical hypersensitivity (Fig. 2, L to N). Blocking the function of female sex hormones through ovariectomy or by antagonizing estrogen receptor signaling using fulvestrant abolished mT_{reg} cell expansion–mediated antinociceptive efficacy (Fig. 2, O to Q). Mice that had undergone ovariectomy and received both estrogen and progesterone supplements—but not either hormone individually—reinstated nociception thresholds comparable to the thresholds of those mice that had not undergone ovariectomy (Fig. 2, O to Q). On the basis of our findings, we concluded that there was a consistent sex hormone–dependent contribution of mT_{reg} cells to the modulation of mechanical hypersensitivity.

T_{reg} cells express *Penk*, which encodes the endogenous opioid peptide enkephalin

T_{reg} cells have increased expression of the *Penk* transcript, which encodes for proenkephalin—a peptide precursor of the analgesic Met- and Leu-enkephalin peptides (*16*, *17*). Although *Penk* is expressed in T_{reg} cells found in the nervous system (*18*), whether T_{reg} cell–derived enkephalin is required for controlling nociception is unknown. We reanalyzed public RNA sequencing data of activated T_{reg} cells, resting T_{reg} cells, as well as activated and resting $CD4^+$ $Foxp3^-$ conventional T cells (T_{conv} cells) (*19*). We observed that *Penk* was higher in activated versus resting T_{reg} cells (Fig. 3A). We also examined other opioid ligand and receptor genes but only recorded a very sparse expression of other opioid-related genes among $CD4^+$ T cell subsets (Fig. 3B).

Enkephalin signals predominantly through the delta opioid receptor (δOR), encoded by the *Oprd1* gene, and with lesser affinity through the mu opioid receptor (μOR) (*20*). On the basis of our prior experience defining mechanical hypersensitivity through enkephalin-δOR circuits in the nervous system, we focused on T_{reg} cell expression of *Penk* (*21*). Using published assay for transposase-accessible chromatin with sequencing (ATAC-seq) data (*19*), we observed more accessible chromatin regions in the *Penk* locus in activated T_{reg} cells but not in other CD4+ T cell subsets. Moreover, this was similar to accessible chromatin within the promoter and enhancer regions in the *Penk* locus from cells of the developing forebrain, an established enkephalinergic area of the murine CNS (Fig. 3C). We found that a proportion of mT_{reg} cells were positively stained for Met-enkephalin after cytokine stimulation, but meningeal $CD4^+$ T_{conv} cells and lymphoid T_{reg} cells were not (Fig. 3D). We validated this observation by generating $Penk^{Cre}$;$Rosa26^{tdTomato}$ mice, which fate-labeled cells where *Penk* has been expressed. The frequency of mT_{reg} cells that had expressed *Penk* in naïve mice (Fig. 3E) was similar to the frequency of Met-enkephalin–expressing cells determined by intracellular antibody staining by flow cytometry. Furthermore, very few lymphoid or intravascular T_{reg} cells were labeled by the fate reporter, confirming the tissue-predominant expression of *Penk* by T_{reg} cells (fig. S5, A and B). This suggested that enkephalin may have a role in tissue mT_{reg} cells specifically. Compared with male mice, female mice had greater numbers of fate-labeled enkephalin-positive T_{reg} cells in the meninges but not in the lymphoid organs (Fig. 3F and fig. S5C). Ovariectomy decreased the overall number of mT_{reg} cells as well as the number of *Penk* fate-labeled mT_{reg} cells in female mice (fig. S5, D and E). This distinction suggested that differences in T_{reg} cells between the sexes may be tissue specific.

mT_{reg} cell–derived enkephalin is required for restraining nociception

Enkephalin is rapidly degraded in the blood but persists in the cerebrospinal fluid (CSF) and nervous system tissues (*22*, *23*). Recent evidence has suggested that meningeal immune cell–derived factors regulate behavior through secreted factors in the CSF (*24*, *25*). Furthermore, factors in the CSF can modulate neuronal activity to promote pain (*22*). In mice where mT_{reg} cells were depleted, enkephalin protein was not detected in the CSF; however, treating mice with IL-2 IT increased its protein level in the CSF (Fig. 3G). After SNI, there was an increase in *Penk* transcripts by mT_{reg} cells and also in the proportion of *Penk* fate labeling among mT_{reg} cells (fig. S5, F and G) Analyzing data from the Immunological Genome project (*26*), we found that in vitro T_{reg} cells were the most prominent immune expressors of *Penk* (fig. S5H), and we validated that they could secrete enkephalin upon stimulation (fig. S5I).

To manipulate the enkephalin lineage of immune cells, we generated bone marrow chimeric mice by transplanting $Penk^{Cre}$;$Rosa26^{DTR}$ bone marrow into irradiated, congenically marked wild-type (WT) mice ($Penk DTR^{\Delta heme}$). This strategy enabled a selective DT-induced depletion of hematopoietic enkephalinergic cells and spares nonhematopoietic enkephalinergic cells of the nervous system and the stroma.

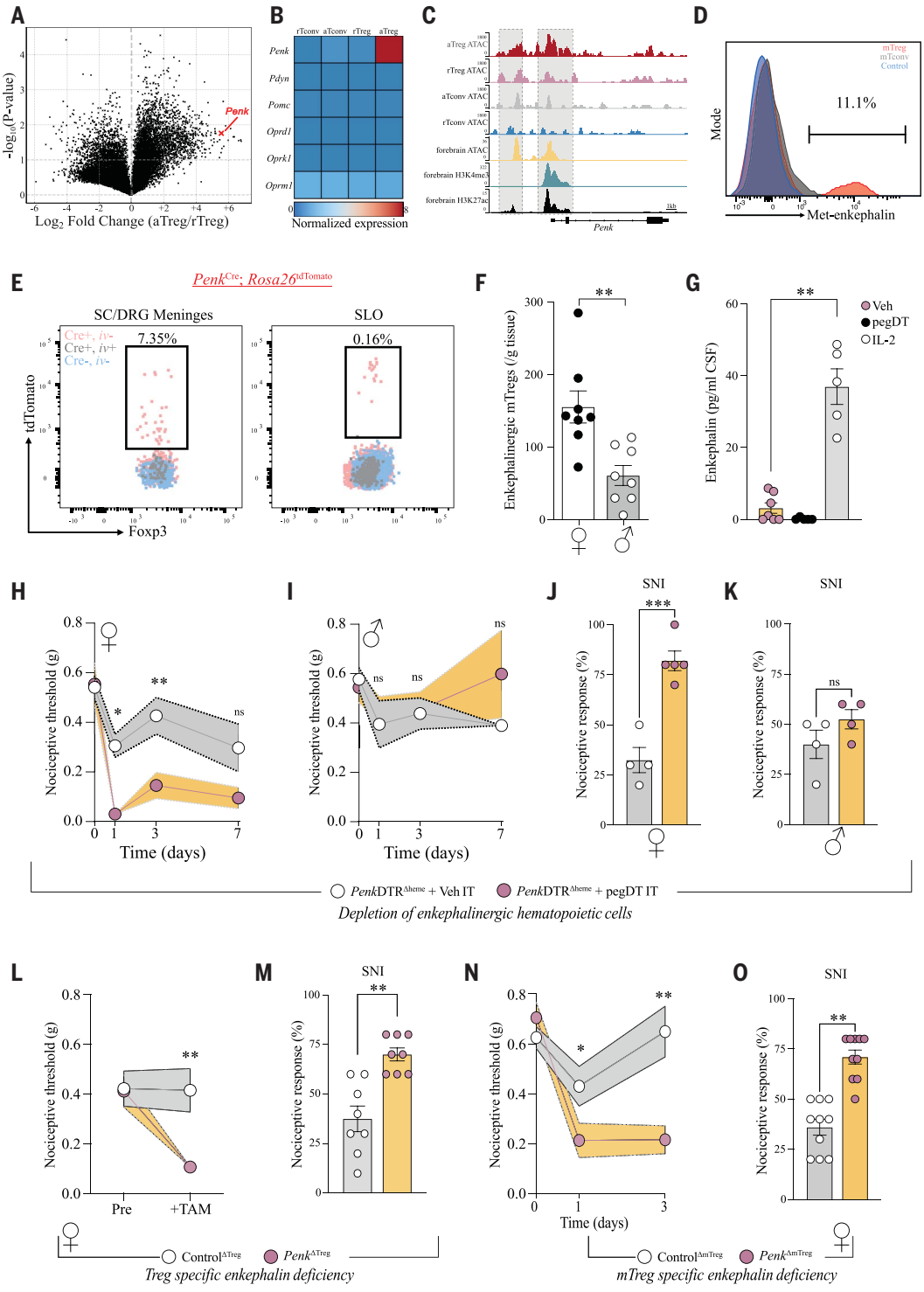

Fig. 3. mT_{reg} cell–derived enkephalin gates nociception. (**A** and **B**) Volcano plot of transcription fold change of activated T_{reg} (aT_{reg}) versus resting T_{reg} (rT_{reg}) cells (A) and heatmap of relative expression value of aT_{reg}, rT_{reg}, and activated and resting $CD4^+$ $CD25^-$ conventional T cells (aT_{conv} and rT_{conv} cells) from public dataset GSE154680 (n = 3) (B). (**C**) Averaged ATAC-seq of open chromatin accessibility peaks on the *Penk* locus in different T cell subsets (n = 4 per group; GSE154680) compared with ATAC-seq and histone modification chromatin immunoprecipitation with sequencing (ChIP-seq) from public ENCODE dataset of the p0 developing forebrain, a known enkephalinergic region. (**D**) Representative stimulated mT_{reg} cells, meningeal $CD4^+$ T cells (mT_{conv} cells) from WT mice, or $Penk^{-/-}$ mT_{reg} cells (control). (**E**) Representative flow cytometry plots (from n = 5 mice) of T_{reg} cells from meninges or secondary lymphoid organs (SLOs) from $Penk^{Cre}Rosa26^{tdTomato}$ mice. Pink represents nonvascular tissue T_{reg} cells from transgenic *Penk* lineage reporter mice, gray represents vascular T_{reg} cells in reporter mice, and blue corresponds to tissue T_{reg} cells from nontransgenic control mice. Gating strategy is provided in fig. S1. (**F**) Number of enkephalin lineage fate reporter–positive tissue mT_{reg} cells in male and female mice; n = 8 mice per group. (**G**) Quantification of enkephalin in mouse CSF after vehicle (pink) IT SLO injection, two pegDT (black) IT injections, or three IL-2 (white) IT injections in *Foxp3*-DTR female mice. Each circle represents samples pooled from five mice with n = 5 to 7 pooled samples per group. (**H** to **K**) Bone marrow chimera of $Penk^{Cre}Rosa26^{DTR}$ bone marrow → WT recipients. Nociceptive thresholds after a single pegDT (pink) or vehicle (white) IT injection in female (n = 4 to 5 mice per group) (H) and male (n = 4 mice per group) (I) mice. Nociceptive response to 0.008 g of von Frey filament after SNI and pegDT (pink) or vehicle (white) IT injection in female (n = 4 to 5 mice per group) (J) and male (n = 4 mice per group) (K) mice. (**L** and **M**) Female $Foxp3^{Cre\text{-}ERT2/Cre\text{-}ERT2}$;$Penk^{fl/fl}$ mice. Nociceptive thresholds of mice before and after tamoxifen injections (L) and percent nociceptive responses after SNI (M). n = 8 mice per group in (L) and (M). (**N** and **O**) Female mixed bone marrow chimeras of *Foxp3*-DTR + $Penk^{-/-}$ (1:1) bone marrow → WT recipients. (N) Nociceptive thresholds of mice after a single pegDT (pink) or vehicle (white) IT; n = 9 to 10 per group. (O) Percent nociceptive responses in SNI mice after pegDT (pink) or vehicle (white) IT injections; n = 10 mice per group. In graphs (F), (G), (J), (K), (M), and (O), individual data points show data for one mouse, and bars show means ± SEMs. In graphs (H), (I), (L), and (N), individual data points show means ± SEMs. Statistics were calculated by unpaired two-tailed Mann-Whitney test [(F), (J), (K), (M), and (O)], Kruskal-Wallis with Dunn's multiple comparisons test (G), or two-way ANOVA with Sidak's test for multiple comparisons [(H), (I), (L), and (N)]. ns, not significant; *P < 0.05; **P < 0.01; ***P < 0.001.

Administering pegDT IT to *Penk*DTR$^{\Delta heme}$ chimeric mice decreased mT$_{reg}$ cell numbers (fig. S5, J to L) and led to a profound female-specific mechanical hypersensitivity in both uninjured and nerve-injured states (Fig. 3, H to K).

Having established a female-specific contribution of hematopoietic enkephalinergic cells to nociception, we used female mice to dissect the mechanism of pain regulation by mT$_{reg}$ cells. To establish whether bone marrow–derived enkephalin was required for the regulation of nociceptive thresholds, we generated chimeric mice in which *Penk*-deficient bone marrow was transplanted into irradiated hosts (*Penk*$^{\Delta heme}$ mice). *Penk*$^{\Delta heme}$ mice displayed decreased mechanical nociceptive thresholds in the uninjured state compared with controls (fig. S5M). Adoptive transfer of *Penk*-sufficient CD4$^+$ T cells into *Rag2*$^{-/-}$ female mice with SNI induced robust antinociception, and deltorphin II, a δOR agonist, successfully reversed the mechanical hypersensitivity that followed mT$_{reg}$ cell depletion (fig. S5, N and O). On the basis of these studies, we concluded that hematopoietic cell–derived enkephalin regulates δOR signaling and was downstream of meningeal T$_{reg}$ cell–derived enkephalin release.

To investigate the contribution of T$_{reg}$ cell–derived enkephalin in mediating mechanical nociceptive thresholds, we generated *Foxp3*$^{Cre\text{-}ERT2/Cre\text{-}ERT2}$;*Penk*$^{fl/fl}$ (*Penk*$^{\Delta Treg}$) mice. Female *Penk*$^{\Delta Treg}$ mice displayed increased mechanical hypersensitivity both in non–nerve-injured and nerve-injured states, which suggests that T$_{reg}$ cell–derived enkephalin controls nociception (Fig. 3, L and M). We generated mice with mixed bone marrow chimeras using a 1:1 ratio of *Foxp3*-DTR and *Penk*$^{-/-}$ bone marrows transplanted into irradiated WT mice. IT pegDT injection into these mice resulted in mT$_{reg}$ cell–specific *Penk* deficiency (*Penk*$^{\Delta mTreg}$ mice) because all *Penk*$^{+/+}$ T$_{reg}$ cells express DTR and are thus ablated by DT administration. Non–nerve-injured, uninjected mixed chimeric mice exhibited similar mechanical thresholds as those of irradiated WT mice transplanted with WT bone marrow (*WT*$^{\Delta heme}$) (Fig. 3N). PegDT IT injection to deplete mT$_{reg}$ cells in *Penk*$^{\Delta mTreg}$ mice increased mechanical sensitivity in uninjured and nerve-injury conditions compared with controls (Fig. 3, N and O). Thus, these data supported the conclusion that mT$_{reg}$ cell–derived enkephalin controls nociception.

T$_{reg}$ cell–derived enkephalin is dispensable for immune suppression

Enkephalin has been linked to skewing of the inflammatory response or tissue injury (*27*, *28*). To test the possibility that T$_{reg}$ cell–derived enkephalin mediates the suppression of nociception by modulating immunological responses, we tested the mechanical nociceptive thresholds of lymphocyte-deficient *Rag2*$^{-/-}$ female mice compared with immunocompetent littermates. We observed decreased mechanical pain thresholds in *Rag2*$^{-/-}$ mice compared with their *Rag2*$^{+/+}$ and *Rag2*$^{+/-}$ littermates (fig. S6A). This finding suggested a mechanism of T$_{reg}$ cell–mediated control of nociceptive thresholds that is independent of lymphocyte-driven inflammation. Because macrophages also contribute to nociception (*29*), we depleted macrophages in mice using liposomal clodronate. Depletion of macrophages did not reverse the mechanical hypersensitivity observed in female mice deficient in mT$_{reg}$ cells (fig. S6B).

Further, we observed no difference in the suppressive capacity of *Penk*$^{-/-}$ T$_{reg}$ cells compared with control T$_{reg}$ cells in suppressing T$_{conv}$ cell proliferation in vitro (fig. S6, C and D). We also did not observe a competitive advantage or disadvantage among *Penk*$^{-/-}$ CD4$^+$ T cells across various tissues after SNI (fig. S6, E to G). There were no differences in effector or regulatory T cell differentiation between the *Penk*-sufficient or -deficient T cells (fig. S6H). Similarly, *Penk*$^{\Delta Treg}$ mice showed no alterations in CD4$^+$ T cell differentiation, spleen size, or weight changes after SNI (fig. S6, I to M).

Using a graft-versus-host disease (GVHD) model, we assessed whether T$_{reg}$ cell–derived enkephalin was required for suppressing immune responses. T helper responses, as judged by the expression of IL-17 or interferon-γ (IFN-γ) by T$_{conv}$ cells, were induced in mice transferred with activated T$_{conv}$ cells in the absence of T$_{reg}$ cells (fig. S6N). Mice that received additional transfers of either *Penk*$^{+/+}$ or *Penk*$^{-/-}$ T$_{reg}$ cells equally suppressed the frequency of T$_{conv}$ cells expressing IL-17A or IFN-γ and mitigated weight loss (fig. S6, N and O). Neither hematopoietic cell–derived enkephalin nor enkephalinergic bone marrow hematopoietic cells were required to restrain T cell differentiation, spleen size, or weight loss after GVHD or SNI (fig. S7, A to H). Rather, we proposed that T$_{reg}$ cells suppressed pain hypersensitivity through a mechanism independent of their role in immunosuppression.

Tissue compartmentalization of sexually dimorphic T$_{reg}$ cell–mediated antinociception

Systemic depletion of T$_{reg}$ cells worsens nociception after nerve injury, regardless of sex (*5*, *6*). *Rag2*$^{-/-}$ female and male mice both demonstrated increased mechanical sensitivity compared with their littermate controls (figs. S6A and S8A). Unlike mT$_{reg}$ cell depletion, which selectively induces hypersensitivity in females, systemic depletion of T$_{reg}$ cells induced hypersensitivity in both sexes in the absence of a nerve injury (fig. S8, B and C). Deficiency of enkephalin in all T$_{reg}$ cells increased mechanical hypersensitivity both before and after nerve injury (fig. S8, D and E). These findings indicated that *Penk* expression in peripheral T$_{reg}$ cells regulated pain sensing independently of sex but that meningeal T$_{reg}$ cell expression of *Penk* regulated nociception only in females.

δOR signaling on MrgprD$^+$ neurons orchestrates the antinociceptive function of mT$_{reg}$ cells

Previously, we have demonstrated a divergence of expression and function of δOR and μOR in mediating distinct pain modalities (*21*). Specifically, the δOR predominates on nonpeptidergic IB4$^+$ unmyelinated as well as myelinated primary afferents and selectively regulates mechanical hypersensitivity (*21*). Conversely, the μOR is expressed on Trpv1$^+$ nociceptors and selectively regulates heat pain hypersensitivity. In addition, spinal δOR-expressing neurons can dampen mechanical hypersensitivity (*30*, *31*). Using a stable cell line expressing the δLight δOR biosensor, an engineered δOR receptor that emits a fluorescent signal upon direct receptor engagement (*20*), we confirmed that deltorphin II and cell culture supernatants from stimulated T$_{reg}$ cells stimulated through their antigen receptor can engage the δOR (Fig. 4A and fig. S9, A to D). By contrast, supernatant taken from stimulated *Penk*$^{-/-}$ T$_{reg}$ cells did not induce a signal from the δOR biosensor (Fig. 4A and fig. S9D). Although selective pharmacological blockade of the δOR by IT injection of naltrindole did not alter mechanical sensitivity in uninjured mice, it diminished the antinociceptive efficacy of IL-2 treatment after SNI (Fig. 4B and fig. S9, E and F).

To assess the role of peripheral nervous system (PNS) or CNS δOR (*Oprd1*) circuits in coordinating the antinociceptive effect of mT$_{reg}$ cells, we intravenously injected δOR-sufficient (*Oprd1*$^{+/+}$) control and *Oprd1*$^{fl/fl}$ mice with adeno-associated viruses (AAVs) that have preferential neurotropism for the PNS or CNS (*32*). This approach selectively introduces Cre recombinase and targets the deletion of δOR in the PNS or CNS, respectively (fig. S9, G and H). We found that δOR deletion in the nervous system compartments did not alter mechanical nociceptive thresholds in uninjured mice, consistent with the existing literature (fig. S9I) (*33*, *34*). However, mice selectively lacking δOR in the PNS, but not the CNS, lost the capacity to respond to the antinociceptive effect of IL-2 post-SNI (Fig. 4, C and D). We concluded that a sensory neuron–expressed, presynaptic δOR mediated mT$_{reg}$ cell suppression of mechanical pain hypersensitivity after nerve injury.

Previous studies of δOR expression in DRG neurons using *Oprd1*^{eGFP} mice have revealed that around half of the reporter-positive cells in the DRGs are myelinated neurons, and ~36% are IB4$^+$ neurons that express the MrgprD receptor (MrgprD$^+$ cells) (*21*). Using published single-cell RNA sequencing data (*35*, *36*), we found that MrgprD$^+$ DRG neurons expressed *Oprd1* and other receptors for ligands expressed by T$_{reg}$ cells (Fig. 4E). We found that 39% of

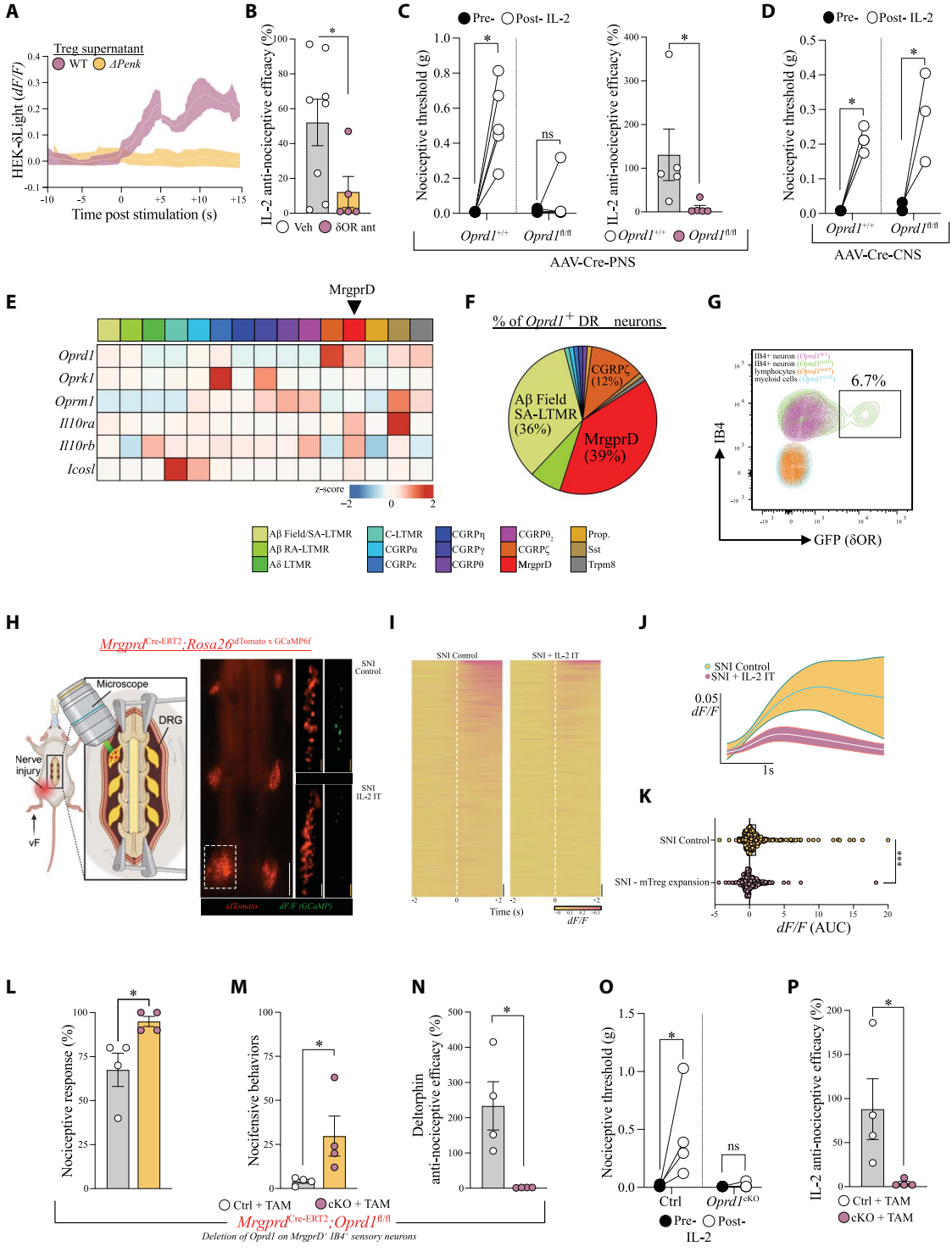

Fig. 4. δOR on MrgprD$^+$ sensory neurons orchestrates mT$_{reg}$ cell–mediated antinociception. (**A**) HEK-δLight activation upon WT (pink) or *Penk*$^{-/-}$ (yellow) T$_{reg}$ cell supernatant application; *n* = 3 biological replicates. (**B**) Antinociceptive efficacy of low-dose IL-2 IT in WT SNI female mice given naltrindole (selective δOR antagonist) or vehicle. Antinociceptive efficacy calculated as ratio of post–IL-2 thresholds compared with preinjury threshold. *n* = 5 to 8 mice per group. (**C**) Nociceptive thresholds and IL-2 antinociceptive efficacy of female mice lacking *Oprd1* in the PNS after mT$_{reg}$ cell expansion compared with controls. *n* = 5 mice per group for all graphs. (**D**) No difference in nociceptive thresholds in female mice lacking *Oprd1* in the CNS after mT$_{reg}$ cell expansion compared with controls. *n* = 3 to 4 mice per group. (**E**) Heatmap of row-normalized expression from DRG sensory neurons clusters from combined GSE139088 and GSE201653. (**F**) Proportions of sensory neuron clusters expressing *Oprd1* from (E). (**G**) Representative flow cytometry plot of δOR-GFP (green) expression on IB4$^+$ MrgprD$^+$ DRG sensory neurons compared with cells from nonreporter mice (purple); *n* = 3 mice. Gating strategy is provided in fig. S9J. Overlaid are lymphoid CD45$^+$ CD90.2$^+$ cells and myeloid CD45$^+$ CD11b$^+$ cells from the DRGs. (**H**) Schematic and representative images of in vivo MrgprD$^+$ sensory neurons of L4 to L6 DRGs showing tdTomato and processed change in GCaMP6 signal after stimulus subtracted by baseline signal

(Δ*F*/*F* intensities) in IL-2–treated SNI mice (n = 4) compared with controls (n = 6). Dashed box represents a whole lumbar DRG shown at 100× magnification on the right. White scale bar, 1 mm; yellow scale bars, 100 μm. (**I**) Heatmap of Δ*F*/*F* neuronal intensities over time of 100 most responsive neurons in IL-2 or vehicle treated SNI mice; 0 represents time of applied von Frey stimulus. Scale bars, 5 neurons. (**J**) Compiled MrgprD$^+$ neuron Δ*F*/*F* time curves post–von Frey stimulus ±90% confidence interval in SNI control (yellow) or mT$_{reg}$ cell–expanded (pink) SNI mice. (**K**) Area under the curve (AUC) values of all individual neurons imaged in the two groups from (J). (**L** to **P**) *Mrgprd*$^{Cre\text{-}ERT2}$; *Oprd1*$^{fl/fl}$ female mice. (L) Percent response to 0.008 g of von Frey fiber stimulation after SNI in female mice. (M) Total nocifensive behaviors (withdrawals, shakes, licks) to 0.008 g of von Frey fiber stimulation after SNI in female mice. (N) Antinociceptive efficacy of deltorphin II (selective δOR agonist) in female mice conditionally lacking δOR on MrgprD$^+$ neurons (pink) or controls (white). (O) Nociceptive thresholds after low-dose IL-2 IT in female mice. (P) Antinociceptive efficacy of low-dose IL-2 IT in female mice. n = 4 mice per group in (L) to (P). In graphs (B), (C), (D), (L), (M), (N), (O), and (P), individual data points show data for one mouse, and bars show means ± SEMs. In graph (K), individual data points show data for one neuron, and bars show means ± SEMs. In graphs (A) and (J), individual data points show means ± SEMs. Statistics were calculated by unpaired two-tailed Mann-Whitney test [(B) and (C); antinociceptive efficacy: (K), (L), (M), (N), and (P)] or Wilcoxon matched-pairs signed rank test [(C); nociceptive threshold: (D) and (O)]. SA-LTMR, slowly adapting low-threshold mechanoreceptor; RA-LTMR, rapidly adapting low-threshold mechanoreceptor; MrgprD, Mas-related G protein–coupled receptor D; Prop., proprioceptor; SST, somatostatin; Trpm8, transient receptor potential cation channel subfamily M member 8; TAM, tamoxifen; cKO, conditional knockout. ns, not significant; *P < 0.05; **P < 0.01; ***P < 0.001.

sensory neurons expressed the *Oprd1* transcript (Fig. 4F), matching previous proportions determined using *Oprd1*^{eGFP} reporter mice (*21*). Profiling the expression of the *Oprd1*^{eGFP} reporter on DRG cells confirmed green fluorescent protein (GFP) expression specifically on IB4$^+$ MrgprD+ sensory neurons. We did not detect *Oprd1*^{eGFP} expression by broadly defined lymphoid and myeloid cells (Fig. 4G and fig. S9J). Sensory neurons, including the IB4$^+$ subset, which were virally encoded to express the δOR biosensor δLight, were capable of δOR activation using Met-enkephalin in vitro (fig. S9, K and L).

Previously, δOR signaling has been shown to suppress voltage-gated calcium channels in presynaptic sensory neurons, including IB4$^+$ sensory neurons (*31*). We generated mice expressing a genetically encoded calcium indicator coupled to a tdTomato reporter in the MrgprD$^+$ sensory neuron population (Fig. 4H). IT administration of IL-2 reduced calcium activity in MrgprD$^+$ neurons in response to von Frey fiber stimulation of the injured hind paw (Fig. 4, I to K, and fig. S9, M to O). We generated mice in which MrgprD$^+$ neurons lacked expression of the δOR (*Oprd1*^{cKO}). Female *Oprd1*^{cKO} mice exhibited exaggerated reflexive and spontaneous nocifensive behaviors after SNI compared with controls but not in the uninjured state (Fig. 4, L and M, and fig. S9P). Furthermore, *Oprd1*^{cKO} female mice with SNI did not respond to the antinociceptive efficacy of deltorphin II and of IL-2 (Fig. 4, N to P). We concluded that mT$_{reg}$ cell–derived enkephalin acted through the δOR specifically expressed by MrgprD$^+$ sensory neurons, mediating the antinociceptive effect of mT$_{reg}$ cells after nerve injury.

Discussion

We describe a sexually dimorphic pain inhibitory circuit between T$_{reg}$ cells residing in the nervous system and sensory neurons. Given the limited number of T$_{reg}$ cells in the healthy, young CNS parenchyma, we refer to the enkephalinergic T$_{reg}$ cell population located in the CNS border tissues as mT$_{reg}$ cells, but we acknowledge their potential ability to migrate between the meninges and the CNS under specific conditions (*37*). Using strategies to deplete or expand T$_{reg}$ cells within the meningeal compartment, we find that mT$_{reg}$ cells gate cutaneous mechanical hypersensitivity by modulating nociceptive processing. The pain-modulating function of mT$_{reg}$ cells is sex selective and regulated by female gonadal hormones.

Although proenkephalin expression by T cells has been identified in various tissues (*16*, *17*), the functional assessment of Met- and Leu-enkephalin in modulating nociception by altering sensory neuron activity has been limited. Recent work has highlighted potential avenues for bidirectional communication between T$_{reg}$ cells and sensory neurons (*38*, *39*). We conclude that mT$_{reg}$ cell–secreted enkephalin acts on δORs on primary sensory neurons to selectively reduce neuronal calcium activity and mechanical hypersensitivity. Our analysis uncovered a sensory modality–selective function of mT$_{reg}$ cells, consistent with prior findings of δOR agonism, specifically providing relief of mechanical but not heat hypersensitivity (*21*). In line with both human and rodent studies, we found that antagonizing or depleting the δOR in the absence of injury or inflammation did not alter mechanical sensitivity, which suggests that there is no endogenous δOR-mediated control of nociception in the absence of nerve injury (*33*, *40*). This suggests that there are other mechanisms to control pain sensing in the naïve state, such as alternative *Penk* peptide splicing by homeostatic T$_{reg}$ cells, engagement of other opioid receptors by enkephalin at steady state, or the need for an inflammatory stimulus to drive δOR trafficking at the neuronal cell surface (*41*).

The engagement of δOR on MrgprD$^+$ sensory neurons by mT$_{reg}$ cell–derived enkephalin selectively reduced mechanical hypersensitivity after tissue insult or nerve injury. T$_{reg}$ cells may further suppress nociception through parallel pathways within peripheral injured tissues (*6*, *35*, *38*). Our findings illustrate a sexually dimorphic pain regulatory mechanism driven by the adaptive immune system and establish mT$_{reg}$ cells as key regulators of endogenous opioid tone and nociceptive processing.

REFERENCES AND NOTES

1. A. M. Aloisi *et al*., *Pain* **132**, S60–S67 (2007).
2. R. E. Sorge *et al*., *Nat. Neurosci.* **18**, 1081–1083 (2015).
3. J. L. Astarita *et al*., *Clin. Exp. Immunol.* **211**, 176–183 (2023).
4. N. Arpaia *et al*., *Cell* **162**, 1078–1089 (2015).
5. J. G. Lees, S. S. Duffy, C. J. Perera, G. Moalem-Taylor, *Cytokine* **71**, 207–214 (2015).
6. M. Davoli-Ferreira *et al*., *Pain* **161**, 1730–1743 (2020).
7. S. Othy *et al*., *Proc. Natl. Acad. Sci. U.S.A.* **117**, 20088–20099 (2020).
8. J. A. Kuhn *et al*., *eLife* **10**, e69056 (2021).
9. M. M. A. Pereira *et al*., *Nat. Commun.* **8**, 14967 (2017).
10. W. Xie, J. A. Strong, J.-M. Zhang, *eNeuro* **4**, ENEURO.0008-17.2017 (2017).
11. S. R. Chaplan, F. W. Bach, J. W. Pogrel, J. M. Chung, T. L. Yaksh, *J. Neurosci. Methods* **53**, 55–63 (1994).
12. H. Graßhoff *et al*., *Front. Immunol.* **12**, 648408 (2021).
13. J. M. Kim, J. P. Rasmussen, A. Y. Rudensky, *Nat. Immunol.* **8**, 191–197 (2007).
14. C. M. Syrett *et al*., *JCI Insight* **4**, e126751 (2019).
15. A. P. Arnold, X. Chen, *Front. Neuroendocrinol.* **30**, 1–9 (2009).
16. N. Aubert *et al*., *eLife* **13**, RP91359 (2024).
17. H. Shime *et al*., *Proc. Natl. Acad. Sci. U.S.A.* **117**, 20696–20705 (2020).
18. M. Ito *et al*., *Nature* **565**, 246–250 (2019).
19. J. van der Veeken *et al*., *Immunity* **53**, 971–984.e5 (2020).
20. C. Dong *et al*., *Nat. Neurosci.* **27**, 1844–1857 (2024).
21. G. Scherrer *et al*., *Cell* **137**, 1148–1159 (2009).
22. M. Kaag Rasmussen *et al*., *Science* **385**, 80–86 (2024).
23. J. P. Burbach, *Ann. Clin. Biochem.* **19**, 269–277 (1982).
24. K. Alves de Lima *et al*., *Nat. Immunol.* **21**, 1421–1429 (2020).
25. M. M. Santisteban *et al*., *Nat. Neurosci.* **27**, 63–77 (2024).
26. A. Baysoy *et al*., *J. Exp. Med.* **220**, e20222052 (2023).
27. L. Basso *et al*., *J. Neuroinflammation* **13**, 132 (2016).
28. G. Laumet *et al*., *Front. Mol. Neurosci.* **12**, 216 (2019).
29. X. Yu *et al*., *Nat. Commun.* **11**, 264 (2020).
30. D. Wang *et al*., *Neuron* **98**, 90–108.e5 (2018).
31. R. Bardoni *et al*., *Neuron* **81**, 1312–1327 (2014).
32. K. Y. Chan *et al*., *Nat. Neurosci.* **20**, 1172–1179 (2017).
33. G. Corder *et al*., *Science* **341**, 1394–1399 (2013).
34. J. Zhang *et al*., *J. Neurosci.* **42**, 7862–7874 (2022).
35. I. Sankaranarayanan *et al*., *J. Neuroinflammation* **20**, 32 (2023).
36. L. Qi *et al*., *Cell* **187**, 1508–1526.e16 (2024).
37. C. Schläger *et al*., *Nature* **530**, 349–353 (2016).
38. A. Jain *et al*., *Nat. Immunol.* **25**, 1296–1305 (2024).
39. Y. Zhu *et al*., *Science* **385**, eadk1679 (2024).
40. G. Stacher *et al*., *Pain* **34**, 271–276 (1988).
41. C. M. Cahill, A. Morinville, C. Hoffert, D. O'Donnell, A. Beaudet, *Pain* **101**, 199–208 (2003).
42. É. Midavaine *et al*., Meningeal regulatory T cells inhibit nociception in female mice, dataset, Dryad (2025).

ACKNOWLEDGMENTS

Figures were generated with BioRender.com. We thank D. Dubal and her laboratory for the FCG mouse, K. Yackle for *Penk*^{Cre} mice, A. Molofsky for *Foxp3*$^{Cre\text{-}ERT2}$*Rosa26*^{tdTomato} mice, A. Pradhan for *Oprd1*^{eGFP} mice, L. K. Dobbs and A. Zimmer for *Penk*^{flox}, J. Chouinard for HEK293-δLight, and M. Ansonoff for assistance with *Penk*$^{-/-}$ tissue isolation. We thank additional members of the

Basbaum laboratory and UCSF ImmunoX for critical feedback. **Funding:** This study received support from Canadian Institute of Health Research (CIHR) (É.M.); the Fonds de Recherche en Santé-Québec (É.M.); the Sandler Foundation PBBR (É.M. and S.W.K.); the Dermatology Foundation (Career Development Award) (S.W.K.); the Benioff Microbiome Research Program (S.W.K.); a Grunfeld Scholar Award from SFVAMC (S.W.K.); National Institutes of Health (NIH) grant T32AR007175-44 (S.W.K.); São Paulo Research Foundation, 2023/04332-0 (B.C.M.); NIH grant NSR35NS097306 (A.I.B.); and Open Philanthropy (A.I.B.). A.I.D. is supported by an ERC Consolidator Award (ERC-2017 COG 771431), a 2022 Pfizer ASPIRE Global Obesity award, Pfizer no. 70591281, NIH PTE no. 5UM1DK105554-09 sub-award 5000826-5500002717, and BBSRC BB/Y006488/1. **Author contributions:** Conceptualization: É.M., S.W.K.; Critical reagents: L.T., A.I.D., J.E.P.; Funding acquisition: É.M., S.W.K., A.I.B.; Investigation: É.M., B.C.M., J.B., S.R.R., S.W.K.; Methodology: É.M., S.W.K.; Project administration: J.M.B.; Supervision: É.M., S.W.K., A.I.B.; Visualization: É.M., N.P.K., W.L.E., S.W.K.; Writing – original draft: É.M., S.W.K.; Writing – review & editing: É.M., S.W.K., A.I.B. **Competing interests:** The authors declare that they have no competing interests. **Data and materials availability:** All data needed to evaluate the conclusions in the paper are present in the paper or the supplementary materials. Raw data used to generate figures along with the data from the analyses of public datasets are deposited in Dryad (*42*).

SUPPLEMENTARY MATERIALS

science.org/doi/10.1126/science.adq6531
Materials and Methods
Figs. S1 to S9
Table S1
References (*43*–*48*)
MDAR Reproducibility Checklist

Submitted 24 May 2024; resubmitted 11 November 2024
Accepted 6 February 2025
10.1126/science.adq6531